J Electroceram (2009) 22:40–46
DOI 10.1007/s10832-007-9384-z

Flame spray synthesis and characterisation of stabilised ZrO_2 and CeO_2 electrolyte nanopowders for SOFC applications at intermediate temperatures

Andre Heel · Andri Vital · Peter Holtappels · Thomas Graule

Received: 15 March 2007 / Accepted: 29 November 2007 / Published online: 19 December 2007

Abstract Zirconia ($Y_{0.16}Zr_{0.84}O_2$, $Sc_{0.2}Zr_{0.8}O_2$ and $Sc_{0.2}Ce_{0.01}Zr_{0.79}O_2$) and ceria ($Gd_{0.2}Ce_{0.8}O_2$) based electrolyte materials are synthesised at production rates up to 260 g h^{-1} by a liquid-fed one-step flame spray synthesis from water-based solutions, or cost-effective rare earth nitrates with a high water content. It was found that this one-step synthesis, based on an acetylene-supported flame is able to produce phase pure and highly crystalline, nanoscale electrolyte materials. The as-synthesised powders show a cubic lattice structure independent of production rates. Specific surface areas of the powders were adjusted between 20 and 60 m^2 g^{-2}, where the latter is an upper limit for the further processing of the powders in terms of screen printing. The influence of process parameters on morphology, particle size, composition, crystallinity, lattice parameter, shrinkage behaviour and coefficient of thermal expansion of the as-synthesised powders were systematically investigated by transmission electron microscopy (TEM), nitrogen adsorption (BET), X-ray diffraction (XRD) and dilatometry. Electrochemical impedance spectroscopy (EIS) was applied at temperatures between 300 °C and 900 °C and confirmed the high quality and the competitive electrochemical behaviour of the produced powders.

Keywords Electrolyte · Nanoparticles · Flame spray synthesis · Ceria · Zirconia · Scandia · Yttria · Gadolinia

A. Heel (✉) · A. Vital · P. Holtappels · T. Graule
Laboratory for High Performance Ceramics,
EMPA Swiss Federal Laboratories for Materials Testing and Research,
Ueberlandstrasse 129,
8600 Duebendorf, Switzerland
e-mail: andre.heel@empa.ch

1 Introduction

Lowering the operating temperature of solid oxide fuel cells (SOFC) from 800 °C to 1000 °C to intermediate temperatures of around 500–700 °C is currently one of the primary scientific aims in the fuel cell community. This can decrease the thermal requirements of the equipment significantly and will enhance lifetime, which is limited due to diffusion and degradation effects in the SOFC materials. The development of new materials and compositions or nanostructured materials, offer the prospect of high performance at lower operating temperatures. Electrolytes from nanostructured materials can help to manufacture thin but densely sintered gastight electrolyte layers or highly reactive nanoscale interlayers [1, 2].

Several methods have been used for the production of electrolytes or mixed oxide materials in general. Beside the production via wet-phase routes, which often need time-consuming additional processing steps like liquid-solid separation, washing and drying, the solid oxide route is an easy to handle production step [3]. Here, the corresponding oxide materials are mixed in a specific stoichiometry and heat-treatment is necessary to reach a solid solution of the single elements. Especially for high-temperature sintering materials, crystal growth is observed. Intensive and time-consuming milling processes are needed, which additionally can cause strong impurities. A common gas-phase production process is the so-called spray pyrolysis [4], where a liquid solution is sprayed into a furnace at elevated temperatures (around 500–600 °C). However, spray-pyrolysed materials are not produced phase pure. Therefore, a subsequent temperature treatment and additional milling processes are indispensable to grind down the particles.

Several gas-phase production routes have been applied to receive nanostructured materials, but most of them are

afflicted by a low output or the necessity of expensive metal-organic precursors [5–9]. The most promising gas-phase route is based on flame reactors, applied in industry for large-scale production of high purity nanoscale materials like carbon black and oxide materials like silica and titania. Maric et al. [10] showed that ceria but also samaria and gadolinia stabilised ceria can be synthesised at production rates of >500 g h^{-1} from metal-organic materials by combustion chemical vapour condensation. The group of Pratsinis worked intensively in the field of flame-made oxides and mixed oxide materials [11]. Nevertheless, for YSZ a different yttrium content was observed in large and small particles, by using inexpensive yttrium nitrates with a high water content. This effect could be reduced when YSZ was produced by metal-organics, or if the materials undergo an intensive chemically treatment to get low water containing yttrium precursors ($Y(NO_3)_3{\cdot}0.5H_2O$=YN0.5 instead of $Y(NO_3)_3{\cdot}6H_2O$=YN6) or to get metal-organics from carbonates via a time-consuming process.

The focus of the present study is a one-step synthesis of various nanostructured, solid-solution electrolyte powders by use of cost-effective metal-organic or water-based nitrate precursor solutions. The specific surface area (SSA) of the powders was restricted to a value between 20 and 60 m^2/g, due to the fact that preparation methods via screen printing pastes can not handle larger SSA values combined with a high solid loading of 40–50%.

Here, a liquid-fed flame spray synthesis (FSS) is presented, where nanostructured, high-crystalline and phase pure electrolyte powders were synthesised. High molar mixtures of metal-organics and nitrates with high water content, or pure inorganic nitrate precursors, diluted in a water/fuel mixture were used. $Gd_{0.2}Ce_{0.8}O_2$ (10GCO), $Sc_{0.2}Zr_{0.8}O_2$ (10SSZ), $Sc_{0.2}Ce_{0.01}Zr_{0.79}O_2$ (10Sc1CeSZ) and $Y_{0.16}Zr_{0.84}O_2$ (8YSZ) were chosen as the most used or promising candidates.

2 Experimental

2.1 Flame spray synthesis

The flame spray plant consists of a commercially available cutting nozzle (Type 150–200, Pangas, Switzerland) with a centred capillary tube ($\varnothing_i$=1.05 mm and $\varnothing_a$=1.6 mm), surrounded by a circular gap for the dispersing gas (gap width=1.4 mm) and six outlets for the supporting flames ($\varnothing_i$=1.5 mm) at a distance of 3.5 mm from the centre. Further details are given elsewhere [12]. A precursor solution with the desired composition is injected via the centre capillary by a continuously running double syringe pump (PN1610, Postnova Analytics, Germany) and is dispersed into fine droplets by a flow of 35 l min^{-1} of pure oxygen (99.95%, Pangas, Switzerland). For the supporting flames acetylene (13 l min^{-1}, 99.5%, Pangas, Switzerland) and oxygen (17 l min^{-1}, 99.95%, Pangas, Switzerland) are premixed in the nozzle body. A similar design running as a methane burner is described in literature [13]. All gases are controlled by mass flow controllers (EL-Flow, Bronnkhorst, the Netherlands). The produced powders are collected in a baghouse filter system (Friedli AG, Switzerland). Small representative samples (0.5–5 g) can be collected on glass fibre filters ($\varnothing$=150 mm, Whatman, UK).

2.2 Precursor solution preparation

For all precursor solutions the total metal concentration was kept constant at 1.25 M. The zirconia based powders (8YSZ, 10SSZ and 10Sc1CeSZ) were produced by using zirconium *n*-propoxide ($Zr(OC_3H_7)_4$ = ZP, 70 wt% in n-propanol, MaTeck, Germany). Yttrium(III) nitrate hexahydrate ($Y(NO_3)_3{\cdot}6H_2O$ = YN6, 99.9% ABCR, Germany), scandium(III) nitrate tetrahydrate ($Sc(NO_3)_3$ $4H_2O$ = ScN4, 99.9% Auer Remy, Germany) and cerium(III) nitrate hexahydrate ($Ce(NO_3)_3$ $6H_2O$ = CeN6, 99.9% Auer Remy, Germany) were dissolved ultrasonically in dimethylformamide (C_3H_7NO = DMF, 99%, Sigma-Aldrich, Switzerland). These intermediate solutions were added slowly to the water sensitive ZP while stirring the receiver. In all cases, clear solutions without any residuals were obtained.

The precursor solutions for the ceria based powders were prepared by dissolving cerium(III) nitrate hexahydrate ($Ce(NO_3)_3$ $6H_2O$ = CeN6, 99.9% Auer Remy, Germany) together with gadolinium(III) nitrate hexahydrate ($Gd(NO_3)_3$ $6H_2O$ = GdN6, 99.9% Auer Remy, Germany) in a H_2O:DMF mixture in a ratio of 5:1 under stirring conditions.

2.3 Powder characterisation

Shrinkage behaviour of the as-produced powders and the coefficient of thermal expansion (CTE) of sintered samples were determined by dilatometry (Baehr Thermoanalyse DIL802, Germany). Experiments for the shrinkage behaviour were made in air between 25 °C and 1550 °C with a heating rate of 5 K min^{-1} by using an alumina sample holder. The determination of the CTE was carried out in air with a sapphire system in the temperature range of 100–980 °C.

Table 1 Electrolyte powders production rates in g h^{-1} as function of precursor flow.

Precursor flow rate	Production rate in g h^{-1} for			
ml min^{-1}	8YSZ	10SSZ 10	10Sc1CeSZ	10GCO
5	46	43	43	65
20	183	170	171	261

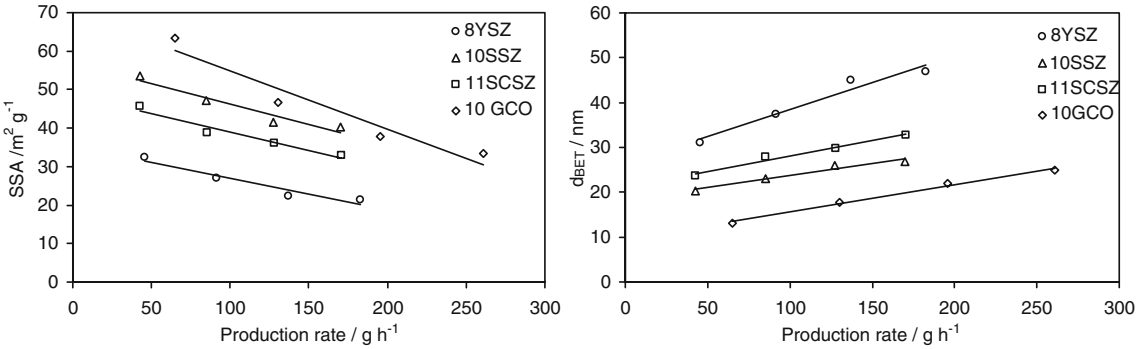

Fig. 1 Specific surface area (*left*) and BET equivalent particle diameter (*right*) of flame spray synthesised solid solution electrolyte materials: 8YSZ (*circle*), 10SSZ (*triangle*), 10Sc1CeSZ (*square*) and 10GCO (*rhombus*). All powders are produced with a constant precursor concentration (1.25 M) with DMF as solvent and a dispersion oxygen flow of 35 l min^{-1}

The crystal structure was analysed by X-ray diffraction (PANalytical X'Pert Pro MPD, Netherlands) with a $Cu{-}K_\alpha$ (λ=1.5405 Å) radiation. Scanning was carried out over a 2θ range of 5–80° with a step size of 0.0167° within a scan time of 150 min. Crystal size was determined by Scherrer equation [14], where K is a constant, β the full width at half maximum value at the Bragg angle (half of the scattering angle 2θ):

$$d_{\mathrm{XRD}} = K\lambda/(\beta\cos\theta) \tag{1}$$

Powder morphology was investigated by high-resolution transmission electron microscopy (HR-TEM; Philips CM30, Netherlands), after heating the powders for 2 h at 473 K in N_2 to remove adsorbed species. SSA was determined by a five-point nitrogen adsorption isotherm at 77 K (SA 3100, Coulter Electronics, USA). The BET equivalent particle diameter d_{BET} can be calculated by assuming monodisperse, spherical and non-aggregated particles:

$$d_{\mathrm{BET}} = 6/(\rho\cdot \mathrm{SSA}) \tag{2}$$

where ρ is defined as the density of the corresponding phase pure composition.

For electrochemical impedance spectroscopy (EIS) an Impedance/Gain-Phase Analyser (Solartron SI 1260, UK) was used. For all material compositions, EIS was carried out in air between 400 °C and 900 °C within a frequency range of 0.1–1 MHz and a signal level of 10 mV. Nanopowders were pressed uni-axially to pellets with a diameter of 15 mm and a height of 1.5 mm. The pellets were sintered afterwards for 2 h at 1550 °C.

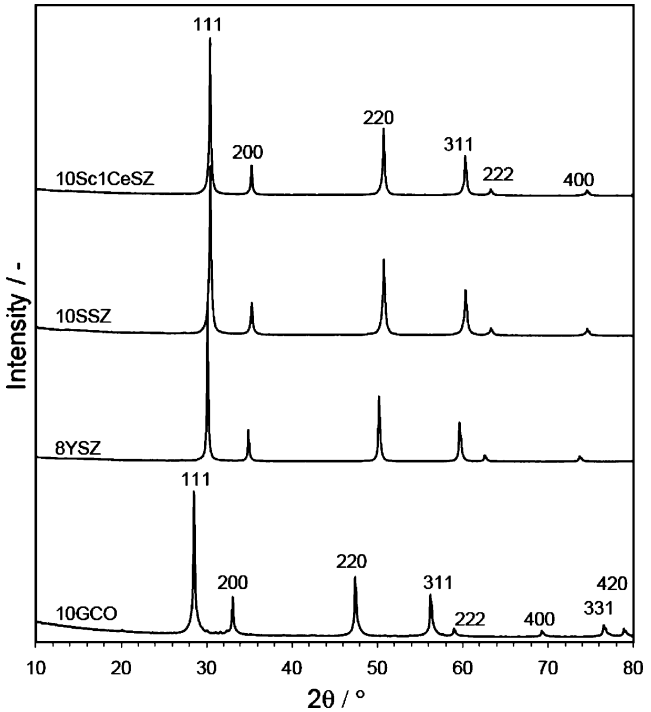

Fig. 2 X-ray diffraction patterns of the as-synthesised powders, prepared with a precursor flow of 5 ml min^{-1}

3 Results

The main control parameters for particle size and morphology are the production rate m_{oxide} in terms of precursor flow, precursor concentration and the amount of dispersing oxygen (V_{O2}). Here the investigation was focused on the influence of m_{oxide}. V_{O2} was constantly kept at a flow rate of 35 l min^{-1}. This corresponds to an overstoichiometry of oxygen for a complete combustion of all species. Additionally, a sufficient high dispersion of the solution during the spraying process can be reached. A more detailed investigation of a general influence of V_{O2} can be found

Table 2 Calculated lattice parameters of the powders and reference values.

Material composition	Crystal structure	a=b=c/ Å	Reference value/Å	Ref.
8YSZ	Cubic	5.139	5.139	[8]
10SSZ	Cubic	5.088	5.091	[15]
10Sc1CeSZ	Cubic	5.090	–	–
10GCO	Cubic	5.426	5.424	[16]

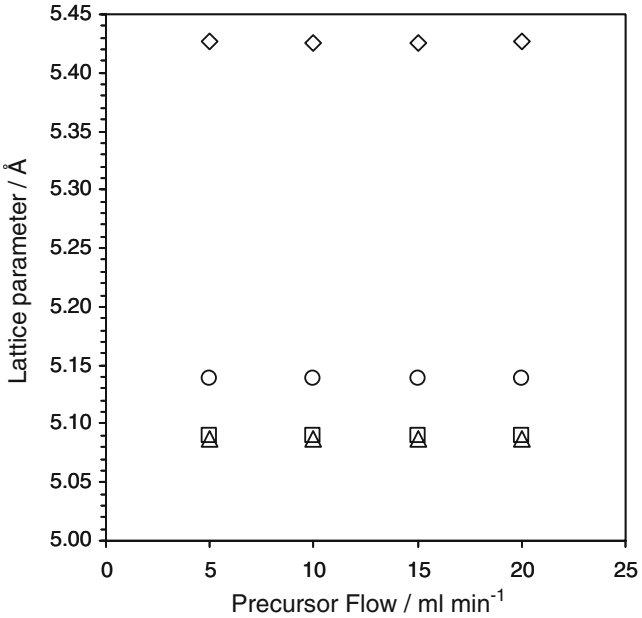

Fig. 3 Influence of powder production rate on the lattice parameter of cubic 8YSZ (*circle*), 10SSZ (*triangle*), 10Sc1CeSZ (*square*) and 10GCO (*rhombus*)

elsewhere [12]. Electrolyte powders were produced from a 1.25 M precursor solution at constant precursor flow rates between 5 and 20 ml min^{-1}, corresponding to production rates between 46 and 261 g h^{-1} in dependence of the material density (Table 1).

With an increasing production rate, the particle size is increasing and the SSA of the powders are decreasing (Fig. 1). While 8YSZ shows the lowest SSA (21–33 m^2 g^{-1}), SSA is increasing for 10Sc1CeSZ (33–46 m^2 g^{-1}) and 10SSZ (40–54 m^2 g^{-1}). For the 10GCO powder a significant higher SSA between 32–64 m^2 g^{-1} can be reached. Due to the high viscosity of the zirconium propoxide (ZP) an increased concentration of ZP results in a higher viscosity of the resulting precursor solution and a reduced atomising effect during the spraying process. Therefore, larger droplets and lower SSA are produced. For 10GCO only pure nitrates in a water/DMF mixture with a viscosity comparable to pure water is used, so that a higher dispersion grade can be reached.

Crystal structure and lattice parameter were determined by X-ray diffraction (XRD) as a function of the production rate. High production rates in combination with high water content in the sprayed precursor can significantly decrease the energy density in the flame. Especially here, the water has to be evaporated and heated up but no combustion enthalpy is released. The reduced flame temperature can cause phase segregation and avoids the synthesis of solid solutions. Independent of the production rate, X-ray diffraction patterns of the as-synthesised material compositions revealed for all powder samples a fluorite-like (cubic) structure (Fig. 2). Beside the cubic reflections no further phases or impurities were observed. The shift of the intensity peaks to smaller diffraction angles, especially for 10GCO, is consistent with an increase of the cubic cell dimension in the order of 10Sc1CeSZ <10SSZ <8YSZ <10GCO. Detailed values calculated from the diffraction patterns are given in Table 2.

The constancy of the lattice parameters of the as-synthesised powders over the precursor flow rate (Fig. 3) demonstrates the applicability of our flame spray synthesis for solid solution materials, even for water-based solutions

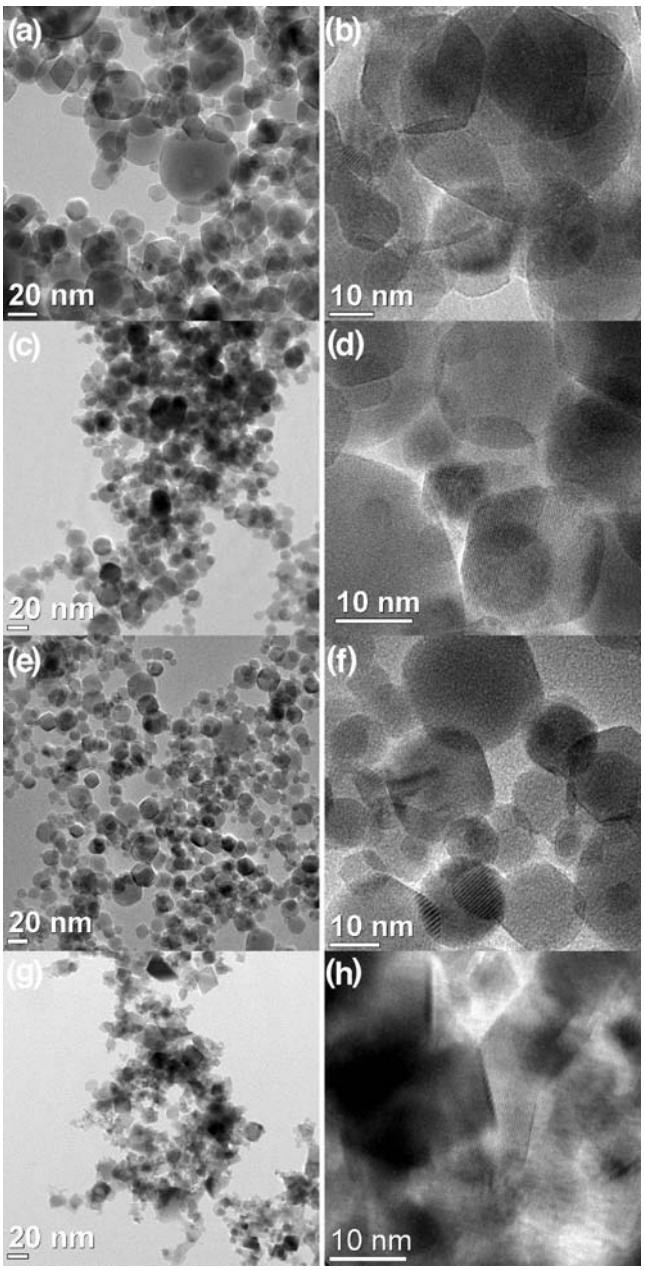

Fig. 4 Overview (*left row*) and HR-TEM image (*right row*) of flame spray made electrolyte powder. From top to bottom: 8YSZ (**a**, **b**), 10SSZ (**c**, **d**), 10Sc1CeSZ (**e**, **f**) and 10GCO (**g**, **h**)

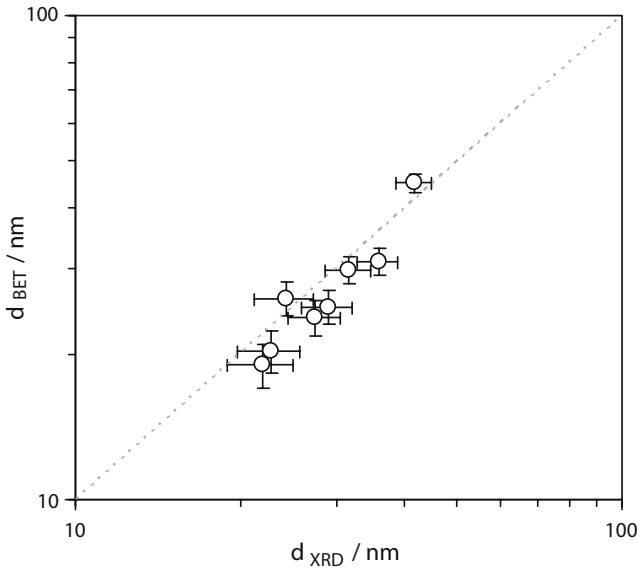

Fig. 5 Comparison of d_{BET} with d_{XRD} of flame spray synthesised electrolyte materials, each for a flow rate of 5 and 20 ml min^{-1}

up to a production rate of 260 g h^{-1}. From the comparison of diffraction pattern and calculated lattice parameter with literature data, it can be suggested that no phase segregation appears and the produced particles are of high quality in terms of phase purity.

From Fig. 4, which gives an overview of the produced particles in a low and high magnification, can be seen, that the zirconia based compositions show spherical-shaped and high-crystalline particles. In contrast to that, 10GCO particles appear rhombic-shaped, as it is well known from ceria based materials [17], however, they show a high crystallinity, too.

HR-TEM images confirmed the observations made by a comparison of average crystallite size (d_{XRD}) with BET equivalent diameter (d_{BET}). In a good agreement with BET data, crystallite size increased with the precursor flow rate,

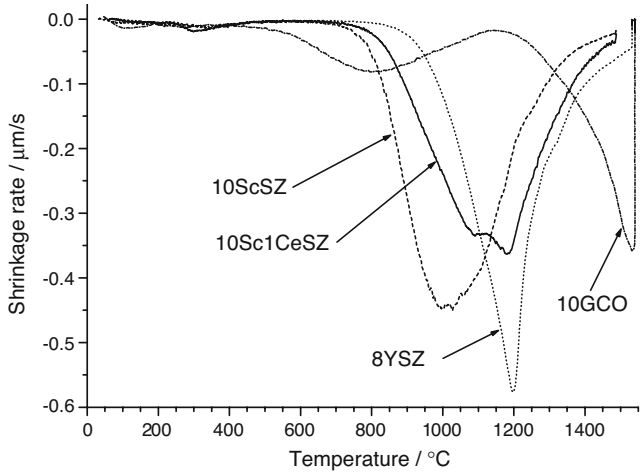

Fig. 6 Shrinkage rate of 8YSZ, 10SSZ, 10Sc1CeSZ and 10GCO as function of temperature

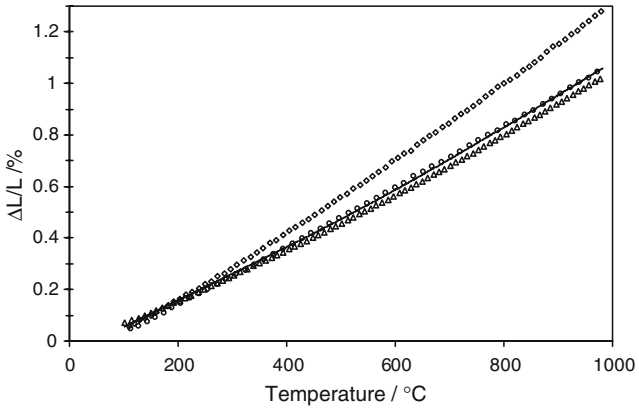

Fig. 7 Relative length change $\Delta L/L$ of 8YSZ (*circle*), 10SSZ (*line*), 10Sc1CeSZ (*triangle*) and 10GCO (*rhombus*) sintered bars (2 h @ 1550°C, sample length: 20 mm)

as it was observed in. Only small deviations of less than 15% could be found between both diameters (Fig. 5). These deviations are in the range of measurement accuracy and also reflect the typical, well known mismatch between XRD and BET data, due to the different weighing of the measurement techniques (volume vs. surface). Nevertheless, from the entire data set can be concluded that the particles are not aggregated and every particle consists of a single crystal.

Figure 6 shows the thermal shrinkage behaviour in terms of the shrinkage rate, which was determined by dilatometry. Compared to usual submicron materials, only a small or negligible shift in the main shrinkage temperature (temperature at the highest shrinkage rate) was observed for all electrolyte powders. Specific surface areas of 25–45 m^2 g^{-1} are too low to show the often discussed influence of the particle size on the shrinkage temperature. The lowest temperature was observed for 10SSZ at 1013 °C, while the addition of already 1 mol% ceria resulted in a higher temperature of 1186 °C. For 8YSZ the highest shrinkage rate was observed at 1198 °C while the 10GCO shows two local maxima at 797 and 1531 °C.

The coefficient of thermal expansion (CTE) of the materials, sintered at 1550 °C for 2 h were calculated from the slope of the relative length change $\Delta L/L$ in two linear regions (Fig. 7): The first region was set from 200 °C to

Table 3 Coefficient of thermal expansion (CTE) for samples of 8YSZ, 10SSZ, 10Sc1CeSZ and 10GCO.

Material composition	CTE/10^{-6} K^{-1} in the temperature range of:		
	200–650 °C	650–980 °C	200–980 °C
8YSZ	11.6	11.6	11.6
10SSZ	10.5	12.3	11.2
10Sc1CeSZ	10.6	12.5	11.4
10GCO	13.8	15.3	14.4

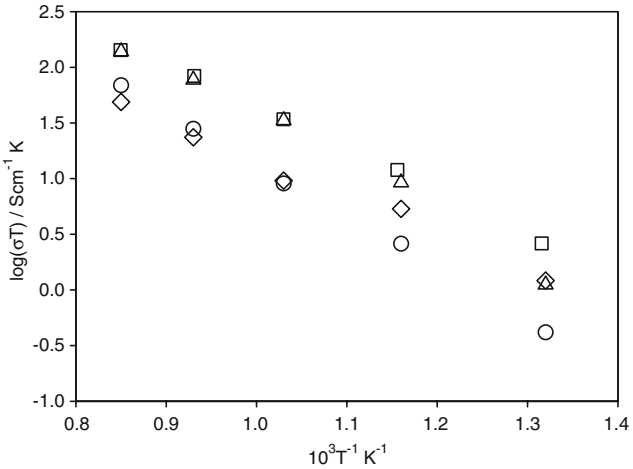

Fig. 8 Arrhenius plot of log(σT) vs. T^{-1} for sintered 8YSZ (*circle*), 10SSZ (*square*), 10Sc1CeSZ (*triangle*) and 10GCO (*rhombus*) samples

650 °C and the second from 650 °C to 980 °C. Additionally, an overall CTE is given for the range from 200 °C to 980 °C (detailed values are given in Table 3). While 8YSZ shows a constant CTE of $11.6 \cdot 10^{-6}$ K^{-1} up to 980 °C, the CTE of the scandia-substituted material (10SSZ) showed a transition from 10.5 to $12.3 \cdot 10^{-6}$ K^{-1}. For 10Sc1CeSZ the same behaviour, but slightly higher values of 10.6 and $12.5 \cdot 10^{-6}$ K^{-1} were observed. Since the as-produced powders definitely show the high-temperature cubic phase, which results from high quenching rates in the flame, the change in the slope can be explained by a phase transition from rhombohedral to cubic [19], caused by the slow heating and cooling rates during sample densification and the dilatometry measurements. Generally higher CTE of 13.8 and $15.3 \cdot 10^{-6}$ K^{-1} were calculated for the 10GCO.

Figure 8 shows the Arrhenius plots of the total conductivity from 500 °C to 900 °C for the given material compositions sintered at 1550 °C for 2 h. The nearly dense pellets had a thickness of about 1.0 mm. The conductivities of the 10SSZ and 10Sc1CeSZ were about 2–5 times higher than that of 10GCO and 8YSZ, respectively. Consistent to literature [20, 21], a change in the slope of the conductivity was observed for 10Sc1CeSZ in the lower temperature region of 550 °C, while 10SSZ still shows significant higher conductivities. In Table 4 total conductivity σ at the particular temperatures of 600 °C and 800 °C is compared to literature data. It can be seen that total conductivity σ of the pellets from the flame spray synthesised powders are on a competitive level for applications at intermediate temperatures. At 800 °C the conductivity of the powders are lower than that of the reference materials, but with a distinct tendency to exceed them. At 600 °C, 10SSZ and 10Sc1CeSZ showed pronounced higher conductivities, while 8YSZ and 10GCO still revealed slightly lower performances. This can be explained by remaining porosities in the sintered pellets: For 8YSZ and 10GCO only 90%, but for 10SSZ and 10Sc1CeSZ 94% of the theoretical density could be reached.

Another aspect, worth to comment here, is the cross-contamination with Si. All powder samples were collected on commercial standard silica filters. It was observed that glass fibres remained in the powders and were sintered with the pellets. Since no Si peaks are observed in the XRD measurements, the amount is rather low or amorphous, but it is well understood that very small contaminations of SiO_2 can decrease the electrochemical performance drastically [22], so that the powder collection process has to be improved.

4 Conclusions

An FSS for nanostructured electrolyte powders is presented. $Gd_{0.2}Ce_{0.8}O_2$, $Sc_{0.2}Zr_{0.8}O_2$, $Sc_{0.2}Ce_{0.01}Zr_{0.79}O_2$ and $Y_{0.16}Zr_{0.84}O_2$ for electrolyte applications at intermediate temperatures (500–700 °C) were successfully synthesised in an acetylene flame at production rates up to 260 g h^{-1} from cost-effective aqueous solutions or nitrates with high water content. The specific surface area of the produced powders met the SSA values restricted to 20–60 m^2 g^{-1} what is a crucial demand for the later processing as screen printing pastes for SOFC applications. Within this range, the specific surface area can easily be adjusted by varying

Table 4 Total conductivity in air at 600 °C and 800 °C for samples of 8YSZ, 10SSZ, 10Sc1CeSZ and 10GCO; sintered at 1550 °C for 2 h.

Material composition	Density %	Total Conductivity/10^{-3} S cm^{-1}				Ref.
		Own experiments[a]		Literature		
		600 °C	800 °C	600 °C	800 °C	
8YSZ	90	3.0	26.3	3.7	67.6	[2]
10SSZ	94	13.8	77.6	9.1	112.2	[23]
10Sc1CeSZ	94	10.7	72.4	7.7	77.6	[21]
10GCO	90	6.1	21.8	9.5	47.8	[17]

[a] Powders are collected on silica filter media.

process parameters like precursor flow, dispersion gas flow or precursor concentration.

The as-synthesised powders showed a high quality concerning solid solution criteria like phase purity, crystallinity and lattice parameters. CTE and conductivity measurements are comparable with literature data and suggest them as high potential materials.

For further improvement of conductivity data, a possible contamination by trace elements has to be considered and chemical purity has to be investigated (e.g. Si from filter media on which powder samples are collected). On the other hand, the sintering process for the pellets has to be adapted to reach higher densities and to avoid residual porosity, respectively.

The FSS showed its applicability for a successful large-scale production of high performance, nanocrystalline electrolyte materials for a wide range of compositions based on cost-effective aqueous solutions with nitrates.

Acknowledgement The authors acknowledge gratefully the funding provided by the European Union in the framework of SOFC600 (SES6-2006020089) and the fruitful discussion with the project partners.

References

1. Y.W. Zhang, Y. Yang, S. Jin, S.J. Tian, G.B. Li, J.T. Jia, C.S. Liao, C.H. Yan, Sol-gel fabrication and electrical property of nanocrystalline (RE2O3)0.08(ZrO2)0.92 (RE=Sc, Y) thin films. Chem. Mater. **13**, 372 (2001)
2. I. Kosacki et al., Electrical conductivity of nanocrystalline ceria and zirconia thin films. Solid State Ion **136–137**, 1225–1233 (2000)
3. J. Sfeir et al., Characterization of perovskite powders for cathode and oxygen membranes made by different synthesis routes. J. Eur. Ceram. Soc. **25**(12), 1991–1995 (2005)
4. P. Holtappels et al., *Perovskite Synthesis by Spray Pyrolysis*, in *Fifth European Solid Oxide Fuel Cell Forum*, ed. by J. Huijsmans (Lucerne, Switzerland, 2002), pp. 103–107
5. A. Heel, G. Kasper, Production and characterization of Pd/SiO2 catalyst nanoparticles from a continuous MOCVS/MOCVD aerosol process at atmospheric pressure. Aerosol Sci. Tech. **39** (11), 1027–1037 (2005)
6. G.L. Messing, S.C. Zhang, G.V. Jayanthi, Ceramic powder synthesis by spray-pyrolysis. J. Am. Ceram. Soc. **76**(11), 2707–2726 (1993)
7. C.H. Chen, K. Nord-Varhaug, J. Schoonman, J. Mater. Syn. Proc. **4**, 189 (1996)
8. F.L. Yuan et al., Preparation of zirconia and yttria-stabilized zirconia (YSZ) fine powders by flame-assisted ultrasonic spray pyrolysis (FAUSP). Solid State Ion **109**(1–2), 119–123 (1998)
9. J. Karthikeyan et al., Nanomaterial powders and deposits prepared by flame spray processing of liquid precursors Nanostruct. Mat. **8** (1), 61–74 (1997)
10. R. Maric et al., Electrolyte materials for intermediate temperature fuel cells produced via combustion chemical vapor condensation. Mater. Manuf. Process. **19**(6), 1143–1156 (2004)
11. R. Jossen et al., Morphology and composition of spray-flame-made yttria-stabilized zirconia nanoparticles. Nanotechnology **16** (6), 609–617 (2005)
12. A. Vital et al., Highly sinter-active (Mg-Cu)-Zn ferrite nanoparticles prepared by flame spray synthesis Acta Mater. **55**(6), 1955–1964 (2007)
13. L. Mädler et al., Controlled synthesis of nanostructured particles by flame spray pyrolysis. Aerosol Sci. **33**, 369–389 (2002)
14. P. Scherrer, Nachr. K. Ges. Wiss. Goettingen, Math.–Phys. Kl. **2**, 98–100 (1918)
15. H. Fujimori et al., Structural changes of scandia-doped zirconia solid solutions: Rietveld analysis and Raman scattering. J. Am. Ceram. Soc. **81**, 2885–2893 (1998)
16. G. Brauer, H. Gradinger, Z. Anorg. Allg. Chem. **276**, 209–226 (1954)
17. D.J. Seo et al., Synthesis and properties of Ce1-xGdxO2-x/2 solid solution prepared by flame spray pyrolysis. Mater. Res. Bull. **41** (2), 359–366 (2006)
18. T. H. Etsell, S.N. Flengas, Electrical properties of solid oxide electrolytes. Chem. Rev. **70**(3), 339 (1970)
19. R. Ruh et al., The System Zirconia-Scandia. J. Am. Ceram. Soc. **60**(9–10), 399–403 (1977)
20. D.S. Lee et al., Characterization of ZrO2 co-doped with Sc2O3 and CeO2 electrolyte for the application of intermediate temperature SOFCs. Solid State Ion **176**, 33–39 (2005)
21. A. Smirnova et al., Scandia-stabilized zirconia: effect of dopants on surface/grain boundary segregation and transport properties. Mater. Res. Soc. Symp. Proc. 972, (2007)
22. C.C. Appel, N. Bonanos, Structural and electrical characterisation of silica-containing yttria-stabilised zirconia. J. Eur. Ceram. Soc. **19**(6–7), 847–851 (1999)
23. D. Lee et al., Characterization of scandia stabilized zirconia prepared by glycine nitrate process and its performance as the electrolyte for IT–SOFC. Solid State Ion **176**, 1021–1025 (2005)